Terahertz spin dynamics driven by an optical spin-orbit torque

Ritwik Mondal,* Andreas Donges, and Ulrich Nowak
Fachbereich Physik, Universität Konstanz, DE-78457 Konstanz, Germany

(Received 12 August 2020; revised 10 February 2021; accepted 8 April 2021; published 14 May 2021)

Spin torques are at the heart of spin manipulations in spintronic devices. Here, we examine the existence of an optical spin-orbit torque, a relativistic spin torque originating from the spin-orbit coupling of an oscillating applied field with the spins. We compare the effect of the nonrelativistic Zeeman torque with the relativistic optical spin-orbit torque for ferromagnetic systems excited by a circularly polarized laser pulse. The latter torque depends on the helicity of the light and scales with the intensity, while being inversely proportional to the frequency. Our results show that the optical spin-orbit torque can provide a torque on the spins, which is quantitatively equivalent to the Zeeman torque. Moreover, temperature-dependent calculations show that the effect of optical spin-orbit torque decreases with increasing temperature. However, the effect does not vanish in a ferromagnetic system, even above its Curie temperature.

DOI: 10.1103/PhysRevResearch.3.023116

I. INTRODUCTION

Interest in controlling spins by means of circularly polarized pulses has grown immensely due to its potential applications in spin-based memory technologies [1–3]. Apart from the heat-assisted spin manipulations, the spins can *also* be controlled using the inverse Faraday effect (IFE) [4–6], the magnetic field of the terahertz pulses [7–10], and an optical spin-orbit torque (OSOT) that does not impart angular momentum into the spin system [11,12]. To be able to explain such effects theoretically, one has to simulate spin dynamics including several nonrelativistic and relativistic effects that might appear at ultrashort timescales [8–12].

The Landau-Lifshitz-Gilbert (LLG) equation of motion, consisting of precession of a spin moment around an effective field and a transverse relaxation, has been used extensively in the past to simulate such spin dynamics [13–15]. However, for a spin system excited by ultrashort laser pulses, a stochastic LLG equation of motion with atomistic resolution is required due to the strong thermal fluctuations to study the dynamical processes [16–20]. In these equations, a stochastic field is added to the effective field to quantify the thermal fluctuations in the spin system. Nonetheless, at ultrashort timescales, the exact form of the LLG equation of motion has to be questioned as several other relativistic phenomena can occur. Therefore, we seek for an equation of motion that can capture all the possible interactions during ultrashort laser excitations of a spin system.

In a previous work, starting from the relativistic Dirac Hamiltonian yet including the magnetic exchange interactions, a rigorous derivation of the LLG equation of motion has been provided [21]. To treat the action of a laser pulse and the corresponding interactions, the Dirac-Kohn-Sham equation with external magnetic vector potential was considered [22–24]. To this end, a semirelativistic expansion of the Dirac-Kohn-Sham Hamiltonian that includes several nonrelativistic and relativistic spin-laser coupling terms was derived [25]. Having these coupling terms, an extended equation of motion that includes *not only* the spin precession and damping *but also* other relativistic torque terms was obtained [26]. One of these torque terms is the field-derivative torque which appears due to the time-dependent field excitation, e.g., in case of THz pulse excitation [27]. Another torque term is the OSOT, which stems from the spin-orbit interaction of the applied field with the electron spins, i.e., it imparts spin-angular momentum of the applied field to the spins. The equation of motion for the reduced magnetization vector $\boldsymbol{m}_i(t)$ including OSOT cast in the form of an LLG equation is

$$\frac{\partial \boldsymbol{m}_i}{\partial t} = -\gamma \boldsymbol{m}_i \times \left(\boldsymbol{B}_i^{\text{eff}} + \boldsymbol{B}_{\text{OSOT}}\right) + \boldsymbol{m}_i \times \left(\mathcal{D} \cdot \frac{\partial \boldsymbol{m}_i}{\partial t}\right). \quad (1)$$

We define the gyromagnetic ratio as γ, and $\mathcal{D}$, representing the damping parameter, is, in general, a tensor. For simplification, we consider only a scalar damping parameter α that can be expressed as $\alpha = \frac{1}{3}\text{Tr}(\mathcal{D})$ [21]. The effective field is represented as $\boldsymbol{B}_i^{\text{eff}}$, which is the derivative of the total magnetic energy without the relativistic light-spin interaction with respect to $\boldsymbol{m}_i$ as will be specified later on in detail. The additional field $\boldsymbol{B}_{\text{OSOT}}$ describes the optomagnetic field induced by the laser pulse due to the OSOT phenomenon.

In this paper, we investigate the effect of the OSOT term within atomistic spin dynamics simulations. First, we revisit the derivation of the OSOT from a general spin-orbit coupling (SOC) Hamiltonian that has been derived within a relativistic formalism [21]. We find that the OSOT depends on the helicity, frequency, and intensity of the light pulse. If the intensity is high and frequency is low, we expect the OSOT terms to show the most significant effects. We simulate the spin dynamics for a spin model, representative for bcc Fe,

*ritwik.mondal@uni-konstanz.de

with the OSOT and find that the OSOT can provide significant contributions at the THz regime. Studying the temperature dependence, we find that the OSOT effect is robust against thermal fluctuations, i.e., we observe no significant reduction of the strength of the OSOT even up to the critical temperature.

II. OPTICAL SPIN-ORBIT TORQUE

The generalized SOC Hamiltonian, as derived within the fully relativistic Dirac framework, can be written as [21,23,26]

$$\mathcal{H}_{\mathrm{SOC}} = -\frac{e\hbar}{8m^2c^2}\,\boldsymbol{\sigma}\cdot[\boldsymbol{E}_{\mathrm{tot}}\times(\boldsymbol{p}-e\boldsymbol{A})-(\boldsymbol{p}-e\boldsymbol{A})\times\boldsymbol{E}_{\mathrm{tot}}], \tag{2}$$

where the electric fields are represented as $\boldsymbol{E}_{\mathrm{tot}} = \boldsymbol{E}_{\mathrm{int}} + \boldsymbol{E}_{\mathrm{ext}}$ and $\boldsymbol{E}_{\mathrm{ext}} = -\frac{\partial \boldsymbol{A}}{\partial t} - \nabla\Phi$ with $(\boldsymbol{A}, \Phi)$ as magnetic vector and scalar potentials. The physical constants have their usual meanings and $\boldsymbol{\sigma}$ denotes the electron's spin through Pauli spin matrices and $\boldsymbol{p}$ is the electron momentum.

Note that the SOC can occur in several ways, as described in the following: (i) the angular momentum of an electron couples to the spin of the electron—this can be expressed as $\boldsymbol{\sigma}\cdot(\boldsymbol{E}_{\mathrm{int}}\times\boldsymbol{p})$, (ii) the first-order magnetic vector potential of the electromagnetic (EM) field couples to the spins—this can be expressed as $\boldsymbol{\sigma}\cdot(\boldsymbol{E}_{\mathrm{int}}\times\boldsymbol{A})$, (iii) the spin angular momentum of the EM field couples to the spin—this can be expressed as $\boldsymbol{\sigma}\cdot(\boldsymbol{E}_{\mathrm{ext}}\times\boldsymbol{A})$.

In a spherically symmetric potential, the first type of SOC can be written as traditional $\boldsymbol{l}\cdot\boldsymbol{s}$ coupling, where $\boldsymbol{l}$ and $\boldsymbol{s}$ represent the orbital and spin angular momentum, respectively. It provides explanations for several relativistic effects in magnetism, e.g., magnetic Gilbert damping [21,28,29] and many others [30,31]. Such a SOC exists even without an external field. On the contrary, the latter two types of SOC depend explicitly on the external field and can be written as

$$\mathcal{H}'_{\mathrm{SOC}} = \frac{e^2\hbar}{4m^2c^2}\,\boldsymbol{\sigma}\cdot[(\boldsymbol{E}_{\mathrm{int}}+\boldsymbol{E}_{\mathrm{ext}})\times\boldsymbol{A}]. \tag{3}$$

The total internal field depends on the intrinsic field $\boldsymbol{E}^0_{\mathrm{int}}$ that even exists without the applied field and the applied field itself. Within the linear response theory we write $\boldsymbol{E}_{\mathrm{int}} = \boldsymbol{E}^0_{\mathrm{int}} + \zeta\boldsymbol{E}_{\mathrm{ext}}$, where ζ defines the coupling strength of the applied EM field relative to the intrinsic one. We thus consider the optical SOC as

$$\mathcal{H}_{\mathrm{OSOC}} = \frac{e^2\hbar(1+\zeta)}{4m^2c^2}\boldsymbol{\sigma}\cdot(\boldsymbol{E}_{\mathrm{ext}}\times\boldsymbol{A}). \tag{4}$$

Using the definition of Zeeman coupling of $-\mu_s\boldsymbol{\sigma}\cdot\boldsymbol{B}_{\mathrm{OSOT}}$, the optical SOC can be shown to induce a field (see Appendix A for details),

$$\boldsymbol{B}_{\mathrm{OSOT}} = \frac{e^2\hbar(1+\zeta)}{4m^2\mu_s}\frac{B_0^2}{\omega}\,\sin\eta\,\hat{\boldsymbol{e}}_x, \tag{5}$$

where $B_0(=E_0/c)$, η, and ω are the envelope of the oscillating Zeeman field (ZF), helicity, and angular frequency of the elliptically polarized light, respectively. μ_s defines the magnetic moment. Note that, due to the OSOT, the induced field points along the direction of the energy flux of the propagating wave. Additionally, note that the field $\boldsymbol{B}_{\mathrm{OSOT}}$ is largest for circularly polarized light ($\eta = \pm\pi/2$). However, if the coupling strength ζ is not the same for right- and left-circularly polarized light, their combined effect could lead to nonzero $\boldsymbol{B}_{\mathrm{OSOT}}$ for linearly polarized light. The parameter ζ depends on the electron density and absorption of the light that can be different for right- and left-circularly polarized light, leading to a magnetic circular dichroism. In the following, we simulate the Zeeman effect from the EM THz field and the optical SOC effects simultaneously, and make a comparison between these two effects in a ferromagnetic system.

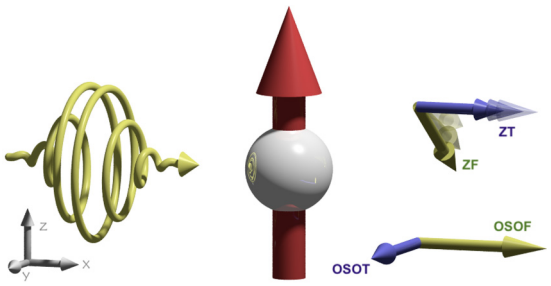

FIG. 1. ZT and OSOT for a single spin (big red arrow) excited by an elliptically polarized laser pulse. The fields and torques are represented by yellow and blue arrows, respectively. Due to the presence of elliptical polarization, the ZF and ZT are drawn as blurry.

III. ATOMISTIC SPIN SIMULATIONS

To compute the spin dynamics, it is convenient to transform the implicit form of our equation of motion to the explicit Landau-Lifshitz (LL) form. For scalar damping parameters, α, the LLG Eq. (1) can be recast as

$$\frac{\partial \boldsymbol{m}_i(t)}{\partial t} = -\frac{\gamma}{(1+\alpha^2)}\boldsymbol{m}_i\times\left(\boldsymbol{B}_i^{\mathrm{eff}}+\boldsymbol{B}_{\mathrm{OSOT}}\right) - \frac{\gamma\alpha}{(1+\alpha^2)}\boldsymbol{m}_i\times\left[\boldsymbol{m}_i\times\left(\boldsymbol{B}_i^{\mathrm{eff}}+\boldsymbol{B}_{\mathrm{OSOT}}\right)\right]. \tag{6}$$

The effective field, $\boldsymbol{B}_i^{\mathrm{eff}}$, is the derivative of total energy with respect to the magnetic moment, $\boldsymbol{B}_i^{\mathrm{eff}} = -\frac{1}{\mu_s^i}\partial\mathcal{H}/\partial\boldsymbol{m}_i$. The LLG equation, Eq. (6), hereby consists of the so-called field-like (see also Fig. 1) and the weaker dampinglike torque which is proportional to the Gilbert damping coefficient $\alpha = 0.01$ and describes the coupling of the spins to a heat bath.

In the following, we consider a spin model for bcc Fe. The total Hamiltonian of the system (without the relativistic spin-light coupling term) $\mathcal{H}$ can be expressed as

$$\mathcal{H} = -\sum_{i<j}J_{ij}\boldsymbol{m}_i\cdot\boldsymbol{m}_j - \sum_i d_z\left(m_i^z\right)^2 - \mu_s\boldsymbol{B}(t)\cdot\sum_i\boldsymbol{m}_i. \tag{7}$$

The first term describes the traditional Heisenberg exchange energy, considering the exchange constants J_{ij} up to the third-nearest neighbor. The second term represents the uniaxial anisotropy with energy constant d_z and the last term is the Zeeman coupling with a time-dependent field $\boldsymbol{B}(t) = \mathcal{R}[\boldsymbol{B}_0\exp(-i\omega t)]$, with a Gaussian shape envelope $\boldsymbol{B}_0 = \boldsymbol{B}_{\mathrm{EM}}\exp(-\frac{t^2}{2\tau^2})$. Following Eq. (5), it is evident that the induced $\boldsymbol{B}_{\mathrm{OSOT}}$ inversely depends on frequency and it has a Gaussian envelope. The ellipticity of the applied pulse is taken into account through $\boldsymbol{B}_{\mathrm{EM}} = \frac{B_{\mathrm{EM}}}{\sqrt{2}}(\hat{\boldsymbol{y}} + e^{i\eta}\hat{\boldsymbol{z}})$, which considers

the major and minor axes of the ellipse and τ defines the pulse duration. In the following, we use the abbreviations Zeeman field (ZF), Zeeman torque (ZT), and optical spin-orbit field (OSOF).

A striking difference between ZT and OSOT is that the ZT does not depend on the frequency of the pulse and is proportional to the amplitude of the applied field pulse. However, the OSOT depends inversely on the frequency and is proportional to the square of the field amplitude, i.e. the intensity. To quantify the OSOT effects, one can estimate its amplitude by computing the characteristic field constant of the OSOF:

$$\tilde{B}(\omega, \zeta) = \frac{4m_e^2 \mu_s \omega}{e^2 \hbar (1+\zeta)}. \tag{8}$$

Considering a central frequency of $f = 1\,\mathrm{THz}$, we find that $\tilde{B}(2\pi f, 0) = 157\,\mathrm{T}$. Hence an EM field amplitude of about 10 T could induce a OSOF of around 1 T, even for the low limit of the coupling strength, $\zeta \to 0$. Needless to mention that the OSOT effects might exceed the ZT if ζ is higher. However, the results shown here were computed for the limit $\zeta \to 0$. Such ultra-intense THz fields are currently only achievable with linear polarization, with recent experiments pointing toward achieving circular polarized laser pulses in the terahertz frequency regime [32,33].

IV. APPLICATION TO FERROMAGNETS

In our following simulations, we consider bcc Fe as a ferromagnetic sample. For the zero-temperature simulations, it is sufficient to solve the LLG equation for a single spin, due to the homogeneity of the THz pulse excitation. The choice of exchange parameters is only relevant at elevated temperatures. We shine an EM pulse having 1 ps pulse duration along the $\hat{\boldsymbol{x}}$ direction with y and z field components as shown in Fig. 1. We will mainly discuss the limit $d_z \approx 0$, since the uniaxial anisotropy does not have a significant impact on the ultrafast spin dynamics (see Appendix B for details).

A. Zero temperature simulations

In particular, we compare the effect of ZT and OSOT at zero temperature. As the optical pulse is applied along the $\hat{\boldsymbol{x}}$ direction ($\boldsymbol{k} = |\boldsymbol{k}|\hat{\boldsymbol{x}}$), we calculate the change in magnetization for y and z components in Fig. 2(a). For the case of only ZT, the induced OSOT obviously remains zero. For a maximum of 10 T applied ZF, the change in magnetization is about 50 % for the y component and 5 % for the z component. The reason for the triggered magnetization dynamics is the following: the ZF from the optical pulse has two components B_y and B_z. The B_y component exerts a torque along $-\hat{\boldsymbol{x}}$ on the equilibrium spin direction,

$$\Delta \boldsymbol{m} \propto m_0 \hat{\boldsymbol{z}} \times B_y \hat{\boldsymbol{y}} = -m_0 B_y \hat{\boldsymbol{x}}, \tag{9}$$

with equilibrium magnetization m_0. On the other hand, the B_z component of the EM field does not exert any torque on the Fe spins at first, as the spins are initially aligned along $\hat{\boldsymbol{z}}$. However, as soon as the above-mentioned torque induced some magnetization Δm_x, the B_z component of the EM pulse, one quarter period later, exerts a torque along the $\hat{\boldsymbol{y}}$ direction:

$$\Delta \boldsymbol{m} \propto \Delta m_x \hat{\boldsymbol{x}} \times B_z \hat{\boldsymbol{z}} = m_0 B_y B_z \hat{\boldsymbol{y}}. \tag{10}$$

Therefore, there exists a superposition between two torques for the ZF. Note that the change in Δm_y magnetization is antisymmetric in the helicity of light, which suggests that the effect is similar to IFE [34]. Further note that the *ab initio* calculations of the IFE were calculated using a nonrelativistic theory [35,36]. However, the present theory is based on a relativistic interaction Hamiltonian. According to Eq. (5), the induced field diverges in the limit $\omega \to 0$, which can be explained by the previous theories of IFE [37–39], and is in accordance with the *ab initio* calculations of IFE [35,36,40]. We would also like to mention that these *ab initio* calculations showed the IFE being asymmetric in helicity for ferromagnets, which includes the absorption of light [36].

The OSOF, on the other hand, has only one component B_x along the $\hat{\boldsymbol{x}}$ direction, see Fig. 2(b). Thus, it exerts a torque along $\hat{\boldsymbol{y}}$-direction

$$\Delta \boldsymbol{m} \propto m_0 \hat{\boldsymbol{z}} \times B_x \hat{\boldsymbol{x}} \propto m_0 B_0^2 \hat{\boldsymbol{y}}. \tag{11}$$

and changes the magnetization by about 50 % as shown in Fig. 2(b). According to our theory in Eq. (5), the right- and left-circular polarization will induce an OSOF along the $+\hat{\boldsymbol{x}}$ and $-\hat{\boldsymbol{x}}$ directions, respectively. Therefore, the right circular pulse exerts a torque along $\hat{\boldsymbol{y}}$ (viz. $\hat{\boldsymbol{z}} \times \hat{\boldsymbol{x}} = \hat{\boldsymbol{y}}$) and, similarly, the left circular pulse exerts a torque along $-\hat{\boldsymbol{y}}$. The change in magnetization is also antisymmetric in the helicity of the light pulse, similar to ZT effects in Δm_y. Note that we have assumed that the material-dependent parameter ζ is zero, which dictates that the antisymmetric behavior is not universal. In fact, the parameter ζ could be different for right- and left-circular pulses, meaning that the antisymmetry of the plots above would be broken [36].

The effective contributions of the combined ZT and OSOT have been computed in Fig. 2(c). We note that the magnetization change in m_y is opposite in helicity for ZT and OSOT [e.g., see fifth row plots in Figs. 2(a) and 2(b)]. Therefore, the final effective contribution becomes only about 5 % change in Δm_y. For the z component of magnetization, the effective Δm_z is negligibly small, even though individual changes are about 5 % due to ZT and OSOT.

To quantitatively understand the ZT and OSOT effects, we compute the field-dependent contributions in terms of the maximum change of each magnetization components Δm_i as a function of the applied field B_0 for left-circular polarized light, shown in Fig. 3. From a simple scaling argument, we would expect the spin excitation $\Delta \boldsymbol{m}_\perp = \Delta m_x \hat{\boldsymbol{x}} + \Delta m_y \hat{\boldsymbol{y}}$ scaling with the magnitude of $\boldsymbol{B}_{\mathrm{EM}}$ and $\boldsymbol{B}_{\mathrm{OSOF}}$, respectively. For the EM field, this is simply the amplitude $\boldsymbol{B}_{\mathrm{EM}} \propto B_0$ whereas, for the OSOF, that is, $\boldsymbol{B}_{\mathrm{OSOF}} \propto B_0^2$ according to Eq. (5).

As already described above, Eq. (9), the spin excitation Δm_x for the EM field is induced by the fieldlike torque from its B_y component, thus, Fig. 3(a) shows a linear scaling with the EM field amplitude B_0. The Δm_y component in Fig. 3(b), however, is induced in a second-order process, described in Eq. (10), and thus scales quadratically with the EM field amplitude B_0, i.e., $\Delta m_y \propto B_0^2$. A deviation of this scaling law is observed at lower field amplitudes of $B_0 \lesssim 100\,\mathrm{mT}$, where the dampinglike torque of the EM field with $\Delta m_y \propto \alpha B_0$ is taking over. This effect can also be seen by comparing the torque amplitudes, which differ by a factor of $\Delta m_y / \Delta m_x \approx \alpha$ in this regime. The Δm_z component, i.e.,

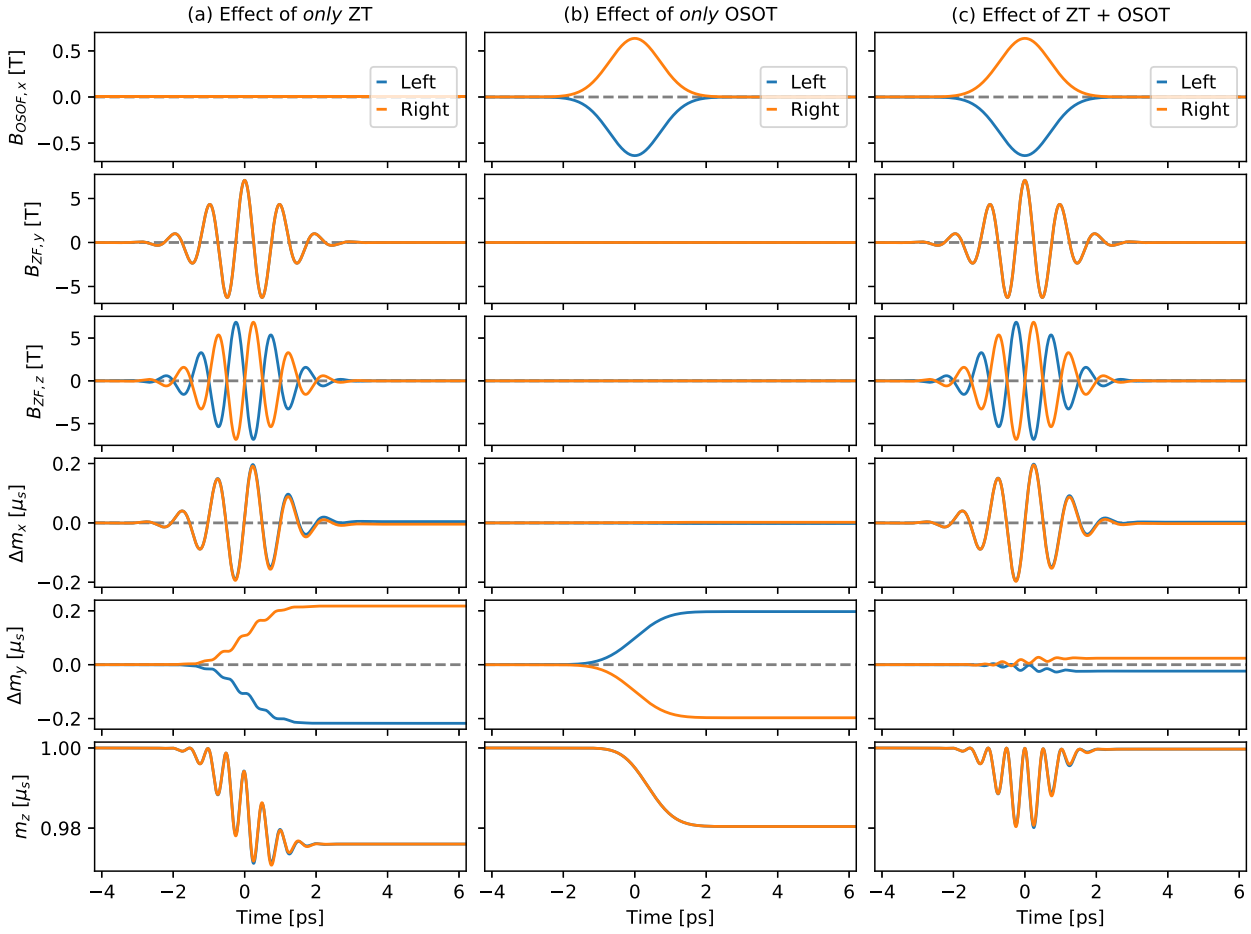

FIG. 2. The dynamical effects of ZT and OSOT for Fe at a maximum applied field of 10 T. The calculations include (a) *only* ZT, (b) *only* OSOT, and (c) both ZT and OSOT. The first row shows the applied ZF which has y and z components, the second row represents the induced OSOF which has only an x component. The other three rows show the change in magnetization along x, y, and z components, respectively.

the deviation of the equilibrium component, then follows from conservation of the magnetization amplitude: $\Delta m_z = m_0 - \sqrt{m_0 - \Delta m_\perp^2}$. At low excitation the dominant contribution here is the Δm_x component and one can simplify $\Delta m_z \approx -\Delta m_x^2/2m_0 \propto -B_0^2$.

In contrast to the EM field, there is only one fieldlike torque acting along the $+\hat{\boldsymbol{y}}$ direction due to the OSOF in the $\hat{\boldsymbol{x}}$ direction. This torque can be seen in Fig. 3(b) and shows the quadratic scaling $\Delta m_y \propto -B_x \propto -B_0^2$ implied by Eq. (11). The Δm_x excitation in Fig. 3(a), on the other hand, is due to the dampinglike OSOT and thus follows the same power law, but a factor of α smaller compared to the fieldlike excitation in Fig. 3(b). Finally, the Δm_z excitation of the OSOT follows again from conservation of magnetization amplitude, leading to $\Delta m_z \approx -\Delta m_y^2/2m_0$ and implying $\Delta m_z \propto -B_0^4$ as shown in Fig. 3(c).

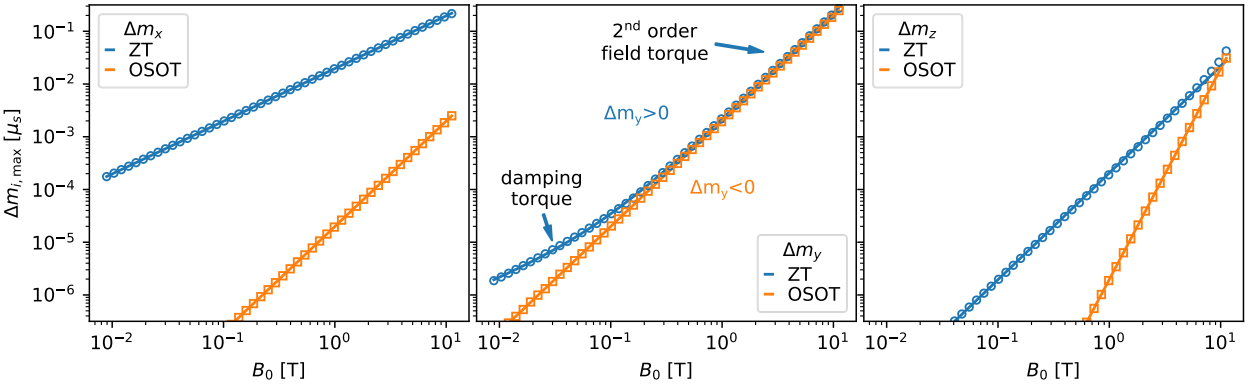

FIG. 3. Maximum of the magnetization change as a function of applied Zeeman field for the application of circular polarized THz pulses (absolute values). Lines are fits to the data according to a single (double) power law, see Table I for coefficients.

TABLE I. Fit parameters to a scaling function $f_N(B_0) = \sum_{n=1}^{N} a_{y,n}(B_0/\mathrm{T})^{\beta_{i,n}}$ where $a_{i,n}$ is given in units of μ_s. For the ZF fit of Δm_y, a double power law $N = 2$ has been used, whereas for the remaining fits a monomial $N = 1$ was sufficient.

		ZF		OSOF	
	n	$a_{i,n}$	$\beta_{i,n}$	$a_{i,n}$	$\beta_{i,n}$
Δm_x	1	$1.975\,924 \times 10^{-2}$	1.00306052	9.898×10^{-5}	1.99910498
Δm_y	1	8.8026×10^{-4}	0.95948487	$1.978\,03 \times 10^{-3}$	1.99858149
	2	$1.743\,23 \times 10^{-3}$	2.09038341	–	–
Δm_z	1	2.0343×10^{-4}	2.03214753	1.96×10^{-6}	3.99720447

These scaling observations are once more summarized in Table I, where we display the scaling exponents obtained by fitting our simulation data. An interesting observation here is that although the characteristic field of the OSOT is on the order of 100 T in this frequency regime, due to the different torque symmetry compared to the ZT, the OSOT is by no means negligible. For the Δm_y excitation, we find that the strength of ZT and OSOT are comparable, though opposite in signs, at fields on the order of 10^2 mT—a value that is in much closer reach experimentally. Altogehter, the OSOT effects can thus provide an equivalent torque compared to the Zeeman effect. Therefore, the OSOT effects cannot be neglected when a circularly polarized light acts on a magnetic system even at the weak coupling limit $\zeta \to 0$.

Up to now, we did not take into account the role of a finite anisotropy. To investigate this, we performed the same calculation depicted in Fig. 2 with the anisotropy $d_z = 7.659\,\mu$eV for Fe included. We found that the main effect of the anisotropy field is the precession of the induced magnetization $\Delta \boldsymbol{m}_\perp$ around the z axis over time (see Appendix B for details). On the other hand, no direct effect of the anisotropy can be observed on the ultrafast timescales, i.e., on the timescale of the pulse duration.

B. Finite temperature simulations

For the finite temperature simulations, the exchange parameters of Pajda *et al.* [41] are used, where the first two nearest neighbors are strongly ferromagnetic, however, the third-nearest neighbor is weakly antiferromagnetically coupled. For these simulations, we also use the uniaxial anisotropy of $d_z = 7.659\,\mu$eV along the z axis to align the magnetization. Calculating the temperature dependence of the OSOT for ferromagnetic Fe, we use a simulation grid of 48^3 spins and add a stochastic field to the effective field in Eq. (6) to treat the thermal fluctuations [17]. The calculated Curie temperature of this system is $T_C = 1368$ K and thus slightly higher than the true value of Fe. However, since the Curie temperature is the only temperature scale in our simulations, we can basically treat it as a free scaling parameter.

We compare in Fig. 4 the OSOT effects at $T = 0$ and $T = 0.73 \times T_C$ (0 K and 1000 K). We find in Fig. 5 that though the OSOT effect in Δm_i appears to decrease with increasing temperature, this reduction is only related to the thermal reduction of magnetic order $m_{eq}(T)$ at finite temperature. In other words, the rotation angle of the normalized magnetization is not sensitive to the temperature.

To illustrate this further, we have systematically calculated the temperature dependence of the OSOT by calculating the difference between maximum spin excitation for right- and left-circular pulses in Fig. 5. For each temperature, we performed ten simulations for each circular pulse and took the average to determine $\max[\Delta m_{R,y}] - \max[\Delta m_{L,y}]$ as a function of temperature, which ensures that the thermal fluctuations are minimized. Far away from T_C, the spin excitation amplitude is proportional to the equilibrium magnetization curve. Only in the close vicinity of the critical temperature, we find an increase of the net spin excitation, relative to the equilibrium magnetization. This is simply due to the large amplitude of both ZF and OSOF, which induce a transient magnetic order.

Therefore, OSOT effects should be observed for bcc Fe even at elevated temperatures i.e., at realistic conditions for ultra-intense spin excitations.

V. CONCLUSIONS

To conclude, we incorporated a torque into the LLG equation that should appear in ultrafast spin dynamics, namely, OSOT, and investigated this effect via computer simulations of an atomistic spin model, representative for bcc Fe. The OSOT originates from the SOC of the electron spins to an external EM field. The strength of this OSOT, unlike the first-order ZT, depends on the *intensity* of the ultrafast light pulse, as well as on the frequency. In addition, the

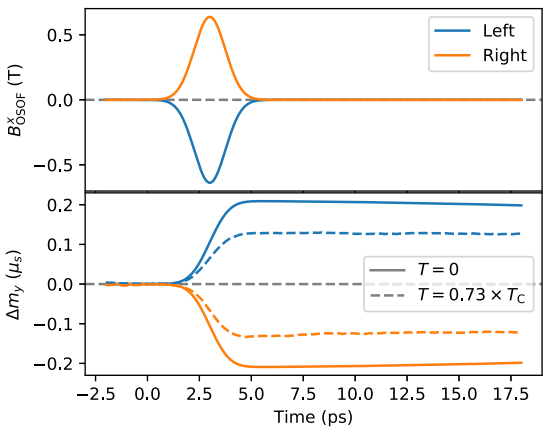

FIG. 4. OSOT effects at finite temperature. Top panel: The OSOT-induced field. Bottom panel: The corresponding spin dynamics for the change of m_y at $T = 0$ and $T = 0.73 \times T_C$ (0 K and 1000 K).

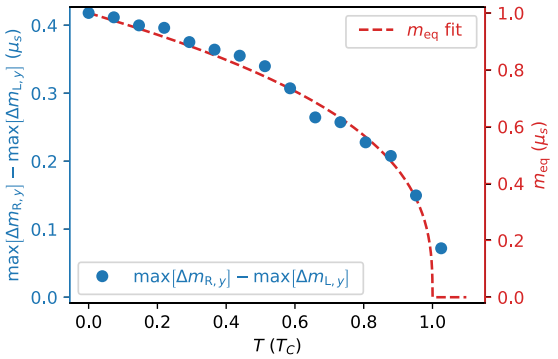

FIG. 5. Temperature dependence of OSOT, by the difference between the maximum changes of m_y due to right and left polarized light pulses at maximum Zeeman field amplitude of 10 T. For comparison, the right axis shows the equilibrium magnetization.

OSOT depends on the ellipticity of the pulse and it provides maximum torque for circularly polarized light pulses. Throughout the simulations presented here, we considered the weak coupling limit $\zeta \to 0$. However, the coupling depends on the electronic configurations of the system and could potentially further increase the strength of the OSOT. Although the OSOT is a higher order contribution in the external field, we found that the ZT and the OSOT provide quantitatively equivalent torques on the spins for circularly polarized laser pulses in the magnetization component perpendicular to the $\boldsymbol{k}$ vector and equilibrium magnetization $\boldsymbol{m}_0$. The effect of the OSOT resembles an already known effect, namely, the IFE and it can be considered as a relativistic contribution to the IFE. The temperature-dependence study of OSOT shows that the OSOT effect is present at elevated temperatures, even up to the Curie temperature.

ACKNOWLEDGMENTS

We thank László Szunyogh for valuable discussions and acknowledge financial support from the Alexander von Humboldt-Stiftung, Zukunftskolleg at Universität Konstanz via Grant No. P82963319 and the Deutsche Forschungsgemeinschaft (DFG) via Project No. NO 290/5-1.

APPENDIX A: DERIVATION OF OPTICAL SPIN-ORBIT TORQUE

Following Eq. (4), the induced field can be written as

$$\boldsymbol{B}_{\mathrm{OSOT}} = -\frac{e^2\hbar(1+\zeta)}{4m^2c^2\mu_s}(\boldsymbol{E}_{\mathrm{ext}} \times \boldsymbol{A}). \tag{A1}$$

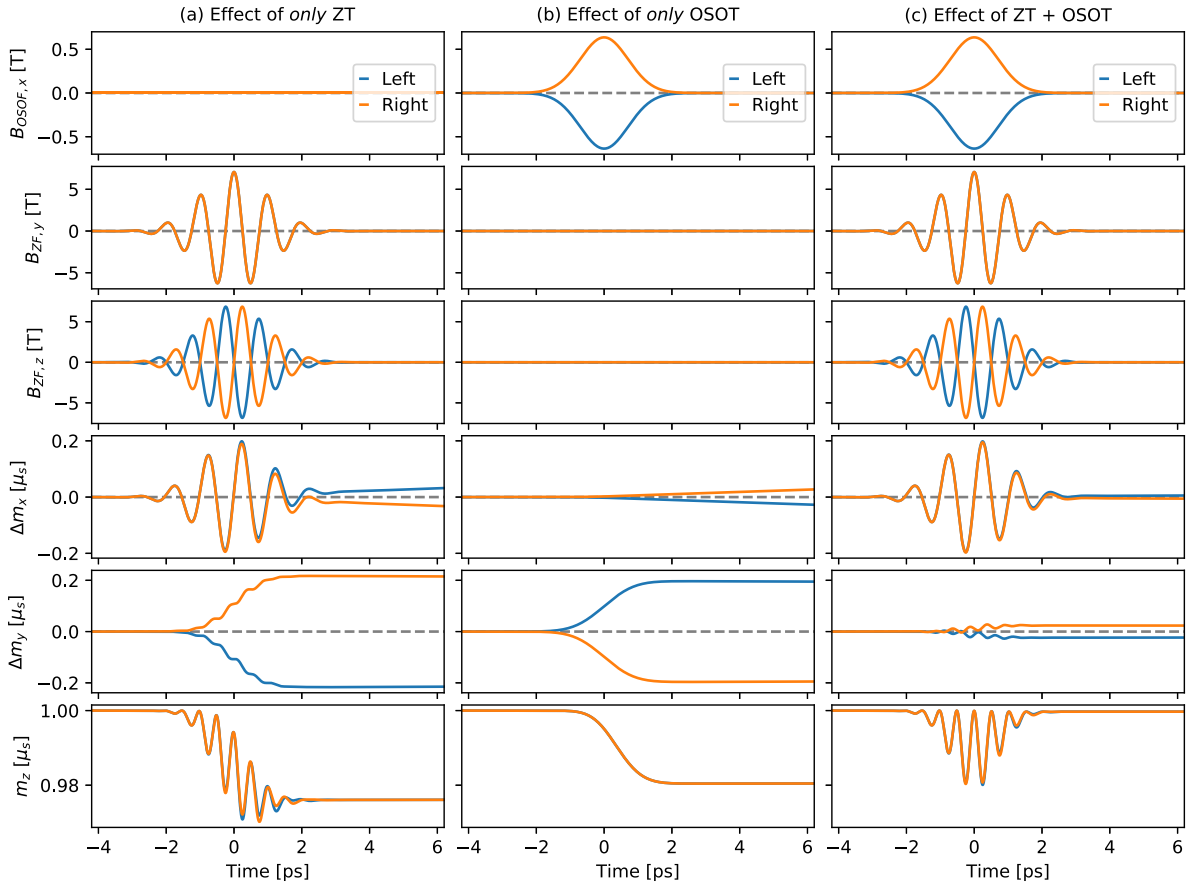

FIG. 6. The dynamical effects of ZT and OSOT have been calculated for Fe including the uniaxial anisotropy at an applied field of 10 T. The calculations have been performed accounting (a) *only* Zeeman effect, (b) *only* OSOT effect and (c) both Zeeman and OSOT effects. In all plots, the first row represents the induced spin-orbit field which has only x component, and rows two and three show the applied ZF which has y and z components. The other three rows show the change in magnetization along x, y, and z components, respectively. The orange and blue colors represent the action of right- and left-circular pulses.

We use the time-dependent field as $\boldsymbol{E}_{\rm ext} = \mathcal{R}(\boldsymbol{E}_0 e^{i(\boldsymbol{k}\cdot\boldsymbol{r}-\omega t)})$ and the amplitude as the elliptically polarized light $\boldsymbol{E}_0 = \frac{E_0}{\sqrt{2}}(\hat{\boldsymbol{y}} + e^{i\eta}\hat{\boldsymbol{z}})$, with η as the ellipticity of the light. Therefore, the electric field can be written as (when only the time-dependent part is taken) $\boldsymbol{E}_{\rm ext} = \frac{\partial \boldsymbol{A}}{\partial t} \Rightarrow \boldsymbol{A} = -\int \boldsymbol{E}_{\rm ext}\, dt$ that can be calculated as follows:

$$\boldsymbol{A} = -\mathcal{R}\left[\boldsymbol{E}_0 \int e^{-i\omega t} dt\right] = -\mathcal{R}\left[i\frac{\boldsymbol{E}_0 e^{-i\omega t}}{\omega}\right]. \tag{A2}$$

Therefore, the induced field can be taken from Eq. (A1) as

$$\begin{aligned}\boldsymbol{B}_{\rm OSOT} &= \frac{e^2\hbar(1+\zeta)}{4m^2c^2\mu_s\omega}\mathcal{R}[i(\boldsymbol{E}_0 \times \boldsymbol{E}_0^{\star})] \\ &= \frac{e^2\hbar(1+\zeta)}{4m^2c^2\mu_s\omega} E_0^2 \sin\eta\, \hat{\boldsymbol{x}} \\ &= \frac{e^2\hbar(1+\zeta)}{4m^2\mu_s\omega} B_0^2 \sin\eta\, \hat{\boldsymbol{x}} \end{aligned} \tag{A3}$$

In the last step of the calculation, we used the relation $E_0 = cB_0$. In our simulations, we apply time-dependent Zeeman fields along y and z directions and the corresponding induced optical spin-orbit field acts along x-direction.

APPENDIX B: EFFECT OF ANISOTROPY

Here, we compute the influence of uniaxial magnetic anisotropy on the spin dynamics induced by the ZT and OSOT. Figure 6 shows the magnetization dynamics, taking into account the uniaxial anisotropy for bcc Fe. The main effect of anisotropy can be noticed by comparing with the zero-anisotropy simulations in Fig. 2. A small increase in Δm_x is observed in the case of only ZF or OSOF after the pulse has passed. This is due to the slow precession of the induced Δm_y component which starts to precess around the anisotropy field along the $\hat{\boldsymbol{z}}$ axis. In the case of the superposition of ZF and OSOF, the excitation of Δm_y is mostly compensated and therefore no Δm_x emerges either. Additionally, we mention that the anisotropy energies do not affect the Δm_y and Δm_z on the ultrafast timescale and the net excitation remains the same irrespective of the anisotropy—at least for the typically weak magnetic anisotropies of the 3d ferromagnets.

[1] A. V. Kimel, A. Kirilyuk, and Th. Rasing, Femtosecond opto-magnetism: Ultrafast laser manipulation of magnetic materials, Laser Photonics Rev. **1**, 275 (2007).

[2] C. D. Stanciu, F. Hansteen, A. V. Kimel, A. Kirilyuk, A. Tsukamoto, A. Itoh, and Th. Rasing, All-Optical Magnetic Recording with Circularly Polarized Light, Phys. Rev. Lett. **99**, 047601 (2007).

[3] A. V. Kimel, A. Kirilyuk, P. A. Usachev, R. V. Pisarev, A. M. Balbashov, and Th. Rasing, Ultrafast non-thermal control of magnetization by instantaneous photomagnetic pulses, Nature (London) **435**, 655 (2005).

[4] R. John, M. Berritta, D. Hinzke, C. Müller, T. Santos, H. Ulrichs, P. Nieves, J. Walowski, R. Mondal, O. Chubykalo-Fesenko, J. McCord, P. M. Oppeneer, U. Nowak, and M. Münzenberg, Magnetisation switching of FePt nanoparticle recording medium by femtosecond laser pulses, Sci. Rep. **7**, 4114 (2017).

[5] S. Mangin, M. Gottwald, C-H. Lambert, D. Steil, V. Uhlíř, L. Pang, M. Hehn, S. Alebrand, M. Cinchetti, G. Malinowski, Y. Fainman, M. Aeschlimann, and E. E. Fullerton, Engineered materials for all-optical helicity-dependent magnetic switching, Nat. Mater. **13**, 286 (2014).

[6] C-H. Lambert, S. Mangin, B. S. D. Ch. S. Varaprasad, Y. K. Takahashi, M. Hehn, M. Cinchetti, G. Malinowski, K. Hono, Y. Fainman, M. Aeschlimann, and E. E. Fullerton, All-optical control of ferromagnetic thin films and nanostructures, Science **345**, 1403 (2014).

[7] M. Shalaby, A. Donges, K. Carva, R. Allenspach, P. M. Oppeneer, U. Nowak, and C. P. Hauri, Coherent and incoherent ultrafast magnetization dynamics in 3d ferromagnets driven by extreme terahertz fields, Phys. Rev. B **98**, 014405 (2018).

[8] T. Kampfrath, A. Sell, G. Klatt, A. Pashkin, S. Mährlein, T. Dekorsy, M. Wolf, M. Fiebig, A. Leitenstorfer, and R. Huber, Coherent terahertz control of antiferromagnetic spin waves, Nat. Photonics **5**, 31 (2011).

[9] T. Kampfrath, K. Tanaka, and K. A. Nelson, Resonant and nonresonant control over matter and light by intense terahertz transients, Nat. Photonics **7**, 680 (2013).

[10] S. Wienholdt, D. Hinzke, and U. Nowak, THz Switching of Antiferromagnets and Ferrimagnets, Phys. Rev. Lett. **108**, 247207 (2012).

[11] N. Tesarová, P. Nemec, E. Rozkotová, J. Zemen, T. Janda, D. Butkovicová, F. Trojánek, K. Olejnik, V. Novák, P. Maly, and T. Jungwirth, Experimental observation of the optical spin-orbit torque, Nat. Photonics **7**, 492 (2013).

[12] G.-M. Choi, J. H. Oh, D.-K. Lee, S.-W. Lee, K. W. Kim, M. Lim, B.-C. Min, K.-J. Lee, and H.-W. Lee, Optical spin-orbit torque in heavy metal-ferromagnet heterostructures, Nat. Commun. **11**, 1482 (2020).

[13] L. D. Landau and E. M. Lifshitz, On the theory of the dispersion of magnetic permeability in ferromagnetic bodies, Phys. Z. Sowjetunion **8**, 153 (1935) [Ukr. J. Phys. **53**, 14 (2008)].

[14] T. L. Gilbert, A phenomenological theory of damping in ferromagnetic materials, IEEE Trans. Magn. **40**, 3443 (2004).

[15] H. Kronmüller and M. Fähnle, *Micromagnetism and the microstructure of ferromagnetic solids* (Cambridge University Press, Cambridge, 2003).

[16] N. Kazantseva, U. Nowak, R. W. Chantrell, J. Hohlfeld, and A. Rebei, Slow recovery of the magnetisation after a sub-picosecond heat pulse, Europhys. Lett. **81**, 27004 (2007).

[17] U. Nowak, *Handbook of Magnetism and Advanced Magnetic Materials* (Wiley, New York, 2007).

[18] R. F. L. Evans, W. J. Fan, P. Chureemart, T. A. Ostler, M. O. A. Ellis, and R. W. Chantrell, Atomistic spin model simulations of magnetic nanomaterials, J. Phys.: Condens. Matter **26**, 103202 (2014).

[19] S. Wienholdt, D. Hinzke, K. Carva, P. M. Oppeneer, and U. Nowak, Orbital-resolved spin model for thermal magnetization switching in rare-earth-based ferrimagnets, Phys. Rev. B **88**, 020406 (2013).

[20] B. Frietsch, A. Donges, R. Carley, M. Teichmann, J. Bowlan, K. Döbrich, K. Carva, D. Legut, P. M. Oppeneer, U. Nowak, and M. Weinelt, The role of ultrafast magnon generation in the magnetization dynamics of rare-earth metals, Sci. Adv. **6**, eabb1601 (2020).

[21] R. Mondal, M. Berritta, and P. M. Oppeneer, Relativistic theory of spin relaxation mechanisms in the Landau-Lifshitz-Gilbert equation of spin dynamics, Phys. Rev. B **94**, 144419 (2016).

[22] R. Mondal, M. Berritta, K. Carva, and P. M. Oppeneer, *Ab initio* investigation of light-induced relativistic spin-flip effects in magneto-optics, Phys. Rev. B **91**, 174415 (2015).

[23] R. Mondal, M. Berritta, C. Paillard, S. Singh, B. Dkhil, P. M. Oppeneer, and L. Bellaiche, Relativistic interaction Hamiltonian coupling the angular momentum of light and the electron spin, Phys. Rev. B **92**, 100402(R) (2015).

[24] A. Crépieux and P. Bruno, Relativistic corrections in magnetic systems, Phys. Rev. B **64**, 094434 (2001).

[25] R. Mondal, M. Berritta, and P. M. Oppeneer, Signatures of relativistic spin-light coupling in magneto-optical pump-probe experiments, J. Phys.: Condens. Matter **29**, 194002 (2017).

[26] R. Mondal, M. Berritta, and P. M. Oppeneer, Unified theory of magnetization dynamics with relativistic and nonrelativistic spin torques, Phys. Rev. B **98**, 214429 (2018).

[27] R. Mondal, A. Donges, U. Ritzmann, P. M. Oppeneer, and U. Nowak, Terahertz spin dynamics driven by a field-derivative torque, Phys. Rev. B **100**, 060409(R) (2019).

[28] K. Gilmore, Ph.D. thesis, Montana State University, 2007.

[29] K. Gilmore, Y. U. Idzerda, and M. D. Stiles, Identification of the Dominant Precession-Damping Mechanism in Fe, Co, and Ni by First-Principles Calculations, Phys. Rev. Lett. **99**, 027204 (2007).

[30] T. Moriya, Anisotropic superexchange interaction and weak ferromagnetism, Phys. Rev. **120**, 91 (1960).

[31] I. Dzyaloshinsky, A thermodynamic theory of "weak" ferromagnetism of antiferromagnetics, J. Phys. Chem. Solids **4**, 241 (1958).

[32] M. Jia, Z. Wang, H. Li, X. Wang, W. Luo, S. Sun, Y. Zhang, Q. He, and L. Zhou, Efficient manipulations of circularly polarized terahertz waves with transmissive metasurfaces, Light: Sci. Appl. **8**, 16 (2019).

[33] Evan V. Jasper, T. T. Mai, M. T. Warren, R. K. Smith, D. M. Heligman, E. McCormick, Y. S. Ou, M. Sheffield, and R. Valdés Aguilar, Broadband circular polarization time-domain terahertz spectroscopy, Phys. Rev. Materials **4**, 013803 (2020).

[34] P. S. Pershan, J. P. van der Ziel, and L. D. Malmstrom, Theoretical discussion of the inverse Faraday effect, Raman scattering, and related phenomena, Phys. Rev. **143**, 574 (1966).

[35] M. Battiato, G. Barbalinardo, and P. M. Oppeneer, Quantum theory of the inverse Faraday effect, Phys. Rev. B **89**, 014413 (2014).

[36] M. Berritta, R. Mondal, K. Carva, and P. M. Oppeneer, *Ab Initio* Theory of Coherent Laser-Induced Magnetization in Metals, Phys. Rev. Lett. **117**, 137203 (2016).

[37] A. Qaiumzadeh, G. E. W. Bauer, and A. Brataas, Manipulation of ferromagnets via the spin-selective optical Stark effect, Phys. Rev. B **88**, 064416 (2013).

[38] D. Popova, A. Bringer, and S. Blügel, Theory of the inverse Faraday effect in view of ultrafast magnetization experiments, Phys. Rev. B **84**, 214421 (2011).

[39] R. Hertel, Theory of the inverse Faraday effect in metals, J. Magn. Magn. Mater. **303**, L1 (2006).

[40] F. Freimuth, S. Blügel, and Y. Mokrousov, Laser-induced torques in metallic ferromagnets, Phys. Rev. B **94**, 144432 (2016).

[41] M. Pajda, J. Kudrnovský, I. Turek, V. Drchal, and P. Bruno, Ab initio calculations of exchange interactions, spin-wave stiffness constants, and Curie temperatures of Fe, Co, and Ni, Phys. Rev. B **64**, 174402 (2001).